Tensile Behavior of Al_2O_3/FeAl + B and Al_2O_3/FeCrAlY Composites

S.L. DRAPER, B.J.M. AIKIN, and J.I. ELDRIDGE

The feasibility of Al_2O_3/FeAl + B and Al_2O_3/FeCrAlY composites for high-temperature applications was assessed. The major emphasis was on tensile behavior of both the monolithics and composites from 298 to 1100 K. However, the study also included determining the chemical compatibility of the composites, measuring the interfacial shear strengths, and investigating the effect of processing on the strength of the single-crystal Al_2O_3 fibers. The interfacial shear strengths were low for Al_2O_3/FeAl + B and moderate to high for Al_2O_3/FeCrAlY. The difference in interfacial bond strengths between the two systems affected the tensile behavior of the composites. The strength of the Al_2O_3 fiber was significantly degraded after composite processing for both composite systems and resulted in poor composite tensile properties. The ultimate tensile strength (UTS) values of the composites could generally be predicted with either rule of mixtures (ROM) calculations or existing models when using the strength of the etched-out fiber. The Al_2O_3/FeAl + B composite system was determined to be unfeasible due to poor interfacial shear strengths and a large mismatch in coefficient of thermal expansion (CTE). Development of the Al_2O_3/FeCrAlY system would require an effective diffusion barrier to minimize the fiber strength degradation during processing and elevated temperature service.

I. INTRODUCTION

FIBER-reinforced intermetallic and superalloy matrix composites have potential applications in advanced gas turbine engine component applications. FeAl + B (Fe-40Al-0.5B, at. pct) and FeCrAlY (Fe-24Cr-8Al-0.06Y, at. pct) were selected as potential matrix materials. FeAl + B was chosen as a potential matrix due to its ductility, low density, and excellent oxidation resistance. While FeCrAlY also has excellent oxidation resistance, its advantages over FeAl + B include a lower coefficient of thermal expansion (CTE) and higher ductility. Both FeAl + B and FeCrAlY are weak at elevated temperature. Therefore, the elevated-temperature strength of composites containing these matrices will depend largely on the strength of the fiber. Few fibers are commercially available that are both strong and compatible with intermetallics and superalloys from both chemical and thermal expansion standpoints. Single-crystal Al_2O_3 fibers were chosen for this study due to their availability, chemical compatibility, relatively high CTE, high-temperature strength, low density, and excellent creep resistance.

The objective of this research was to assess the feasibility of Al_2O_3/FeAl + B and Al_2O_3/FeCrAlY composite systems for high-temperature applications. The fiber-matrix chemical compatibility and interfacial bond strength in the two systems were investigated. Since fiber strength is crucial to the strength of the composite, Al_2O_3 fiber strengths were determined both prior to and after processing. The tensile responses of the FeAl + B and FeCrAlY matrices, as well as the composites, were characterized. The experimentally measured composite tensile properties were compared to predicted values.

Acoustic emission (AE) instrumentation was used during room-temperature tensile tests to aid in determining the failure mechanisms of the composites. Stress waves, which are emitted during plastic deformation or crack growth, are processed by the AE equipment into AE parameters. Interpretation of the AE parameters can only be done in general terms, but some correlation of AE parameters to damage modes has been established.[1,2] AE signals associated with fiber fractures typically have high amplitudes, in excess of 90 dB,[1,2] whereas those due to matrix cracks and debonding have lower amplitudes. Results of the acoustic emission testing and microstructural analyses of the composites after tensile testing were related to possible failure mechanisms.

II. EXPERIMENTAL PROCEDURE

Prealloyed powders with nominal compositions Fe-40Al-0.5B and Fe-24Cr-8Al-0.06Y (at. pct) were used to fabricate matrix-only and composite plates. The composites were reinforced with three plies of continuous, *c*-axis single-crystal Al_2O_3 fibers, supplied by Saphikon, Inc. (Milford, NH). Fibers were oriented in the 0 deg direction (parallel to the tensile axis). The majority of the fibers procured for this study had a sizing of methyl cellulose for protection during shipping. The sizing was removed by burning or cold-water washing prior to fabrication. However, more recent fibers were purchased in the unsized condition to eliminate the removal process. The unsized fibers were used in the Al_2O_3/FeAl + B composites tested at 700 K. The single-crystal fibers were optimized as this program proceeded such that subsequent batches of fiber had smaller, more uniform diameters and had generally improved strength.

The composites were fabricated by the powder cloth technique.[3] In this technique, the fibers were wound onto

S.L. DRAPER and J.I. ELDRIDGE, Materials Research Engineers, are with the Materials Division, NASA Lewis Research Center, Cleveland, OH 44135. B.J.M. AIKIN, Research Associate, is with the Department of Materials Science & Engineering, Case Western Reserve University, Cleveland, OH 44106.

Manuscript submitted October 19, 1994.

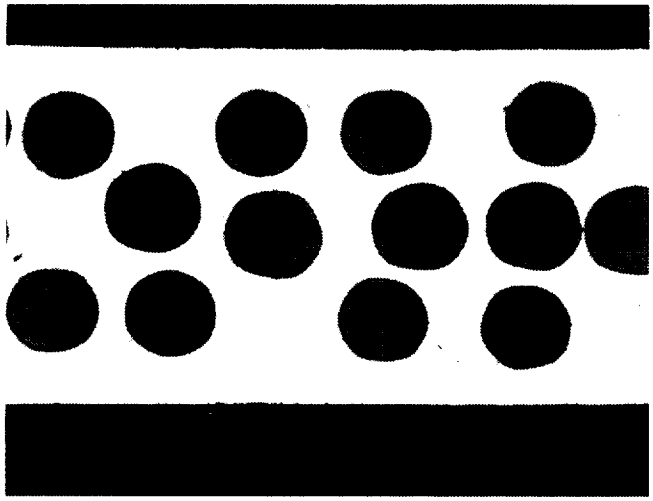

(*a*)

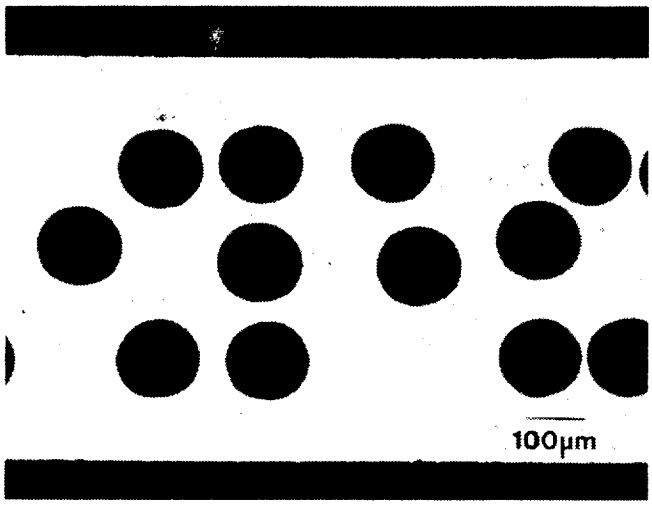

(*b*)

Fig. 1—Typical fiber distributions of as-fabricated (*a*) Al_2O_3/FeAl + B and (*b*) Al_2O_3/FeCrAlY composites.

a lathe, and a poly(methyl methacrylate) (PMMA) binder was applied to form a fiber mat. The matrix powder was mixed with a poly(tetrafluoethylene) (TEFLON*) binder and rolled out into a clothlike sheet. Alternate layers of powder cloth and fiber mat were stacked and consolidated in a vacuum hot press resulting in either a 5 by 15 cm or a 5 by 20 cm plate. Five Al_2O_3/FeAl + B and eight Al_2O_3/FeCrAlY composite plates were fabricated. Monolithic plates were fabricated without binders.

*TEFLON is a trademark of E.I. Du Pont de Nemours & Co., Inc., Wilmington, De.

Interfacial shear strength was measured by the fiber push-out technique at room temperature for both composite systems and at elevated temperatures for Al_2O_3/FeCrAlY. Details of the fiber push-out technique have been described elsewhere.[4,5]

Fibers were etched from the composite plates at room temperature to determine the effect of composite consolidation on fiber strength. The fibers were etched from FeAl + B with a solution of 50 vol pct H_2O, 33 pct HNO_3, and 17 pct HCl. The fibers were removed from FeCrAlY by using a solution of 33 pct HNO_3, 33 pct HCl, and 33 pct H_2O. As-received fibers were similarly etched to determine whether the etching procedure caused damage to the fibers.

Al_2O_3 fibers in the as-received, as-received plus etched, and etched from the composite conditions were tensile tested at room temperature using a crosshead speed of 1.27 mm/min and a gage length of 12.7 mm. The diameters of the fibers were measured using a split image microscope. All error estimates represent 95 pct confidence intervals assuming a Gaussian distribution. The sample sets contained 15 to 20 fibers at room temperature and 6 to 10 fibers at elevated temperatures. Elevated temperature tensile testing of Al_2O_3 fibers was done in air with 5.0 or 7.6 cm of fiber between the grips. The longer fibers were needed to accommodate the furnace, which was made as short as possible to accomplish these tests. The furnace was mounted vertically resulting in a temperature gradient within the furnace. At a temperature setting of 1200 K, the top, center, and bottom temperatures in the 2.54-cm-long furnace were 1080, 1200, and 875 K, respectively. However, the temperature in the center 0.50 cm of the furnace varied by only 20 K. Any fiber failing within the furnace was considered a good test.

Monolithic tensile specimens were machined by wire electrodischarge machining, whereas composite specimens were machined by water jet cutting. Three 14- or 19-cm-long, reduced gage specimens with a 15.2-mm gage length were machined from each plate. Specimen surfaces were polished with SiC paper before testing. The specimens were tested in air at a constant crosshead speed of 0.13 mm/min. Specimens from at least two different plates were tested at each temperature. Strain was measured with an axial extensometer attached to the edges of the specimen.

Acoustic emission data were collected from one room-temperature composite tensile test for each matrix composition. The AE technique detects stress waves emitted by stressed material to detect plastic deformation or crack growth. The stress waves were recorded by the AE equipment, which processed the waveforms into set parameters. Two sensors, with resonant frequencies of 250 kHz, were used to eliminate noise outside the gage length and to locate failure events within the gage section.

Optical microscopy and scanning electron microscopy (SEM) were performed on as-fabricated and tensile-tested samples. Longitudinal metallographic specimens were polished to examine fiber cracks, and transverse sections were polished to examine interfaces and to measure the volume fraction of fibers, V_f. Fracture surfaces of the tested specimens were also examined.

III. RESULTS

A. *Microstructure*

Typical fiber distributions for both composite systems are shown in Figure 1. Fiber volume fractions ranged from 0.18 to 0.31 for Al_2O_3/FeAl + B composite plates and from 0.21 to 0.45 for Al_2O_3/FeCrAlY composite plates. Volume fractions were dependent upon fiber diameter, fiber spacing during winding, and the thickness of the powder cloth. The fibers were fairly uniformly spaced (Figure 1), but binder burn-off during hot pressing can result in fiber movement and subsequent nonuniformity in fiber spacing. The non-

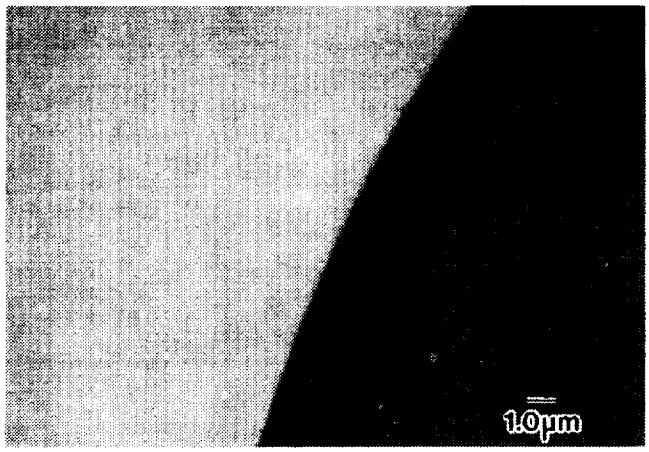

(*a*)

(*b*)

Fig. 2—Microstructure of (*a*) Al_2O_3/FeAl + B and (*b*) Al_2O_3/FeCrAlY interface after annealing at 1250 K for 200 h.

posites were fully consolidated after hot pressing, but second phases, containing interstitials, were located at prior particle boundaries.

Chemical analysis of the composite specimens was performed to determine residual binder content. The F content averaged 244 ppm in the Al_2O_3/FeAl + B samples and 312 ppm in the Al_2O_3/FeCrAlY specimens. Nonzero values of fluorine are indicative of incomplete TEFLON burn-off. The average carbon content of monolithic FeAl + B was 118 ppm but increased to an average of 824 ppm in the Al_2O_3/FeAl + B composites. The high C content in the Al_2O_3/FeAl + B composites was determined to be from incomplete burn-off of the PMMA binder.[6] The average C content in the Al_2O_3/FeCrAlY specimens was 394 ppm. Oxygen contents could not be measured in the composites due to the presence of oxide fibers.

A certain amount of fiber breakage occurred upon fabrication. Visual inspection and nondestructive evaluation showed fiber breakage was clustered in specific areas, which implied that slight deviations in the hot-pressing dies contributed to fiber breakage. The fibers etched from FeAl + B composites were generally broken, with the majority being in the range of 5 to 10 cm in length from a 19-cm-long composite plate, although some fibers maintained the

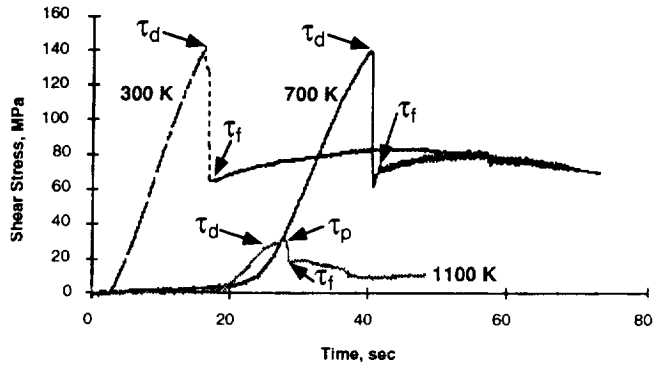

(*a*)

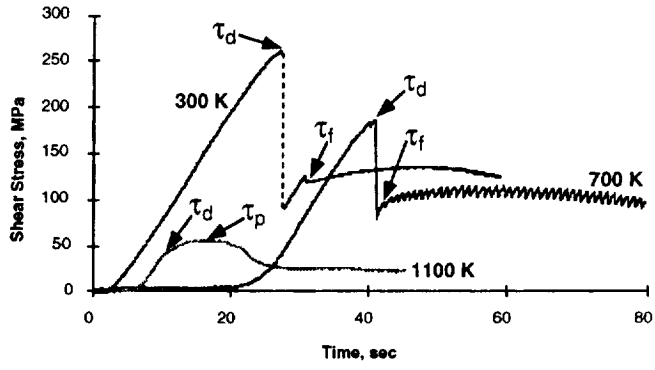

(*b*)

Fig. 3—Typical Al_2O_3/FeCrAlY stress-displacement plots for fiber push-out tests at 298, 700, and 1100 K for (*a*) V_f of 0.45 and (*b*) V_f of 0.33.

19-cm length. The majority of fibers etched from a 19-cm-long FeCrAlY composite plate were greater than 10 cm in length, a few of which were unbroken.

The composites were annealed in flowing argon at 1250 K for 200 hours to determine chemical compatibility between the matrices and fibers. Analysis of the Al_2O_3/FeAl + B sample indicated a significant amount of carbon contamination due to the binder used in processing. During annealing, the C segregated to some of the matrix-fiber interfaces and formed a C-Fe-Al phase. However, the remaining fiber/matrix interfaces were clean, with no reaction product visible by SEM (Figure 2(a)). Aside from the reactions due to C contamination, the Al_2O_3/FeAl + B system showed little or no reaction. Reaction products were observed intermittently around the circumference of the Al_2O_3 fibers in FeCrAlY (Figure 2(b)). The reaction products were less than 1-μm thick after annealing at 1250 K for 200 hours. These reaction products consisted of various ratios of Fe:Cr:Al or Al:Y:Cr.

B. *Interfacial Shear Strength*

Fiber-matrix interfacial shear stresses were determined using the fiber push-out technique. Typical fiber load/displacement curves at 298, 700, and 1100 K tests are shown in Figure 3 for Al_2O_3/FeCrAlY. Generally, a sharp drop in load indicates complete fiber debonding,[4] τ_d. The debonding event is further verified by visual monitoring and by a spike in the acoustic emission signal. The post-debond portion of the load/displacement curve characterizes the frictional shear stress, τ_f. In addition, a peak stress, τ_p,

Table I. Debond and Frictional Shear Strengths

Sample	Temperature (K)	Number of Tests	τ_d (MPa)	τ_p (MPa)	τ_f (MPa)
Al_2O_3/FeAl + B	298	21	55 ± 13	—	21 ± 6
Al_2O_3/FeCrAlY					
V_f = 0.26	298	17	191 ± 18	—	111 ± 10
V_f = 0.45	298	8	143 ± 21	—	68 ± 8
(plate A)	700	6	139 ± 28	—	53 ± 21
	1100	4	30 ± 4	34 ± 4	16 ± 7
V_f = 0.33	298	8	274 ± 25	—	124 ± 16
(plate B)	700	5	183 ± 6	—	83 ± 15
	1100	6	43 ± 7	51 ± 2	—

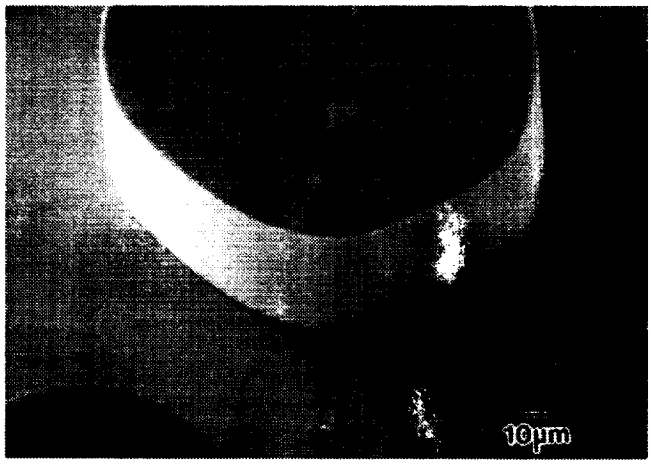

(*a*)

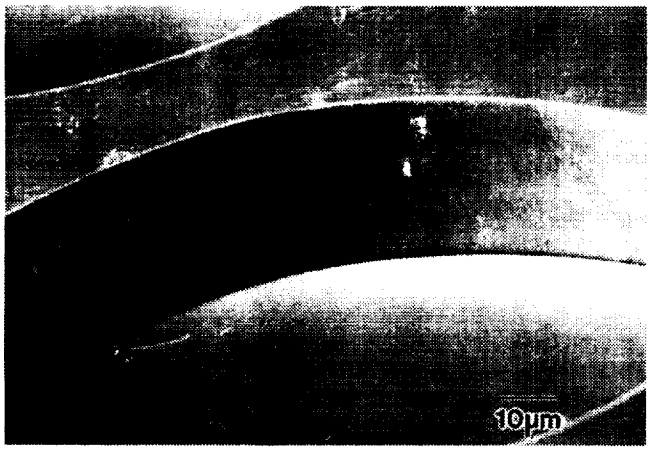

(*b*)

Fig. 4—(*a*) The surface of a pushed-out Al_2O_3 fiber in FeAl + B was smooth as was (*b*) the matrix where a fiber had been pushed out.

after fiber debonding was sometimes observed at elevated temperatures due to matrix yielding, as indicated in Figure 3(b).

Fiber push-out was performed only at room temperature for Al_2O_3/FeAl + B, and the load/displacement curves were similar to that shown in Figure 3(b). The interfacial bonds in Al_2O_3/FeAl + B were quite weak with average strengths of τ_d = 55 ± 13 MPa and τ_f = 21 ± 6 MPa (Table I). Despite the low interfacial strengths, debonding was indicated by load drops and spikes in the AE signal. The pushed-out Al_2O_3 fibers in FeAl + B displayed no adhesion of the matrix to the surface of the fiber (Figure 4(a)), and the surface of the matrix where a fiber had been pushed out was similarly smooth (Figure 4(b)).

The interfacial shear strength of the Al_2O_3/FeCrAlY system was measured on specimens from three different composite plates at room temperature and from two composites plates at elevated temperatures (Table I). The most complete room-temperature push-out data came from a plate with 0.26 fiber volume fraction and resulted in interfacial shear strengths of τ_d = 191 ± 18 MPa and τ_f = 111 ± 10 MPa. The fibers pushed out of Al_2O_3/FeCrAlY had a rough surface due to the adhesion of the matrix (Figure 5(a)). These adhesions caused considerable roughness in the matrix where the fiber had been pushed through (Figure 5(b)). The two plates used for elevated temperature push-out testing, designated plates A and B, were fabricated in the same time period, and the only known difference was fiber volume fraction. Fiber volume fractions averaged 0.45 and 0.33 for plates A and B, respectively. Typical load displacement plots for the two composite specimens are given in Figure 3. Composite plate A had similar interfacial shear strengths at 298 and 700 K (Table I). Composite plate B had a decrease in interfacial bond from 274 ± 25 MPa at room temperature to 183 ± 9 MPa at 700 K. At 1100 K, matrix yielding usually occurred both before and after fiber debonding, resulting in nonlinear loading as well as a peak stress after fiber debonding. Composite plate A had a lower average debond and frictional shear strength at all test temperatures. The differences in interfacial shear strengths between these two plates were significant even though the chemistries of the two plates were similar.

C. *Etched-Out Fiber Strength*

The effect of powder cloth fabrication on Al_2O_3 fiber strength (σ_f) was determined by comparing the strength of as-received fibers to the strength of fibers etched out of one Al_2O_3/FeAl + B and one Al_2O_3/FeCrAlY composite plate. The as-received fibers were taken from the spool just before and after composite fiber winding. A group of fibers was also tested in the as-received plus etched state to ensure that the etching procedure had not damaged the fibers. The strengths of the as-received and as-received plus etched groups were nearly identical so the data were pooled, resulting in an average as-received fiber strength of 2483 ± 343 MPa with a Weibull modulus (m) of 5.6 (Figure 6).

The degradation in fiber strength was severe for the fibers etched from FeAl + B: a 43 pct degradation in strength at room temperature (σ_f = 1413 ± 174 MPa, m = 4.1). Fi-

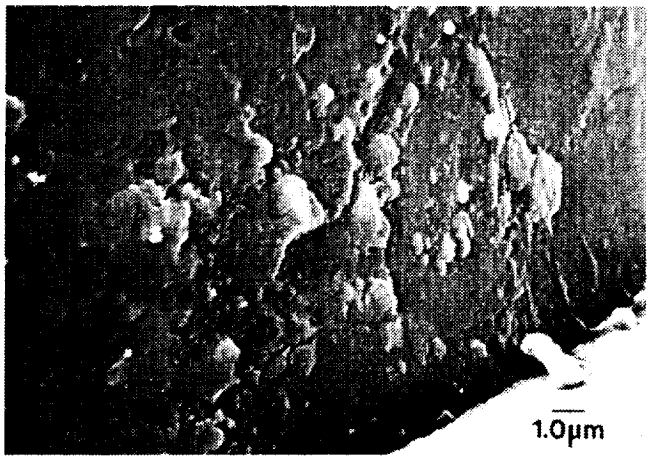

(*a*)

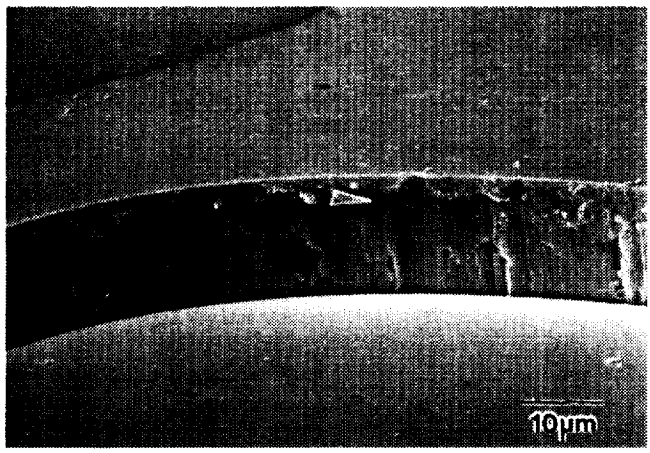

(*b*)

Fig. 5—(*a*) The surface of a Al_2O_3 fiber pushed out of FeCrAlY had an adherent matrix, and (*b*) the matrix where a fiber had been pushed out was grooved.

bers from the same composite plate were also tested at elevated temperatures with maximum furnace temperatures set at 700 and 1100 K (Table II). The strengths of the fibers etched from the composites were determined to be near 610 MPa at both 700 and 1100 K. Compared to the elevated temperature strengths of as-received fibers from a different spool,[7] the strengths of these fibers were degraded by 33 to 50 pct. Particles were observed on the etched-out fiber surfaces, and analyses by X-ray photoelectron spectroscopy concluded they consisted solely of carbon (Figure 7). Electron dispersive spectroscopy analyses of the *in situ* reaction product formed during annealing revealed the presence of Fe and Al as well as C at the interface. This discrepancy could be due to removal of the Fe and Al during the etching procedure or due to formation of a different phase during annealing. The carbon residue was associated with fracture initiation sites on single fiber tensile tests (Figure 7(b)). The association of these deposits with fiber fracture initiation sites indicated that the presence of the carbon residue was detrimental to the fiber strength.

The fibers etched from FeCrAlY had a degradation in strength of 32 pct at room temperature with an average strength of 1693 ± 180 MPa. Similar to the fibers etched from FeAl + B, the fiber strengths degraded by approxi-

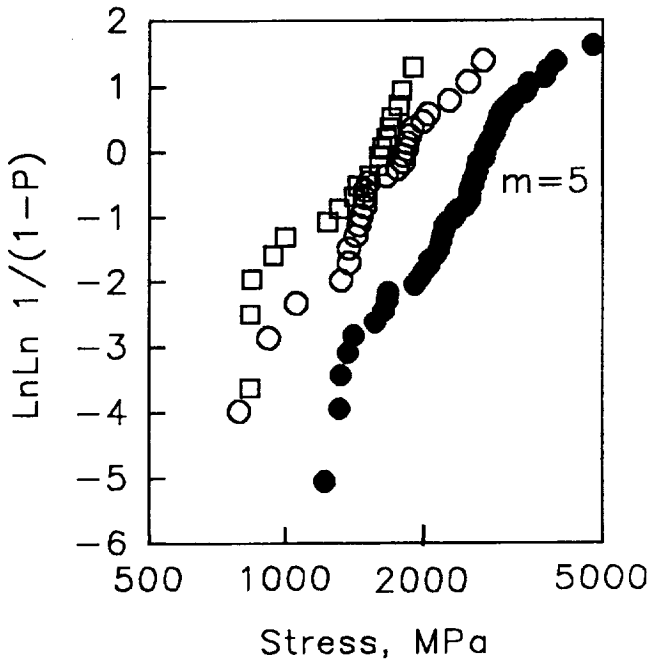

Fig. 6—Weibull plot of as-received fiber (●), which includes as-received plus etched data and fiber etched from FeAl + B (○) and FeCrAlY (□).

Table II. Tensile Strength of Al_2O_3 Fiber Etched from Composite

Matrix	Temperature (K)	Average σ_f (MPa)	Minimum σ_f (MPa)
FeAl + B	298	1413 ± 174	836
	700	610 ± 140	385
	1100	611 ± 84	294
FeCrAlY	298	1693 ± 180	791
	700	809 ± 140	312
	1100	472 ± 270	308
As-received	298	2484 ± 128	1220
As-received[7]	298	3352 ± 243	—
	673	1170 ± 150	—
	1073	926 ± 43	—

mately 30 to 50 pct of the as-received strength at elevated temperatures (Table III). The surface of the Al_2O_3 fibers etched from a FeCrAlY matrix composite had adherent particles that were rich in Cr and Al and deficient in Fe in comparison to the FeCrAlY matrix (Figure 8(a)). In other areas of the fiber surface, a Y-rich phase was observed in grooved areas on the Al_2O_3 fiber surface (Figure 8(b)). These are consistent with the reaction products observed at the interface after annealing at 1250 K for 200 hours.

D. *FeAl + B and Al_2O_3/FeAl + B Tensile Behavior*

1. *FeAl + B*

Typical stress-strain curves for monolithic FeAl + B at 298, 700, and 1100 K are shown in Figure 9. Monolithic FeAl + B had a room-temperature 0.2 pct yield stress (σ_y) of 370 ± 22 MPa and strain hardened to an ultimate tensile strength (σ_{UTS}) of 518 ± 137 MPa. The average σ_y and σ_{UTS} at 700 K were 348 and 542 MPa, respectively, but decreased to 64 and 67 MPa at 1100 K. The average elastic moduli were 204 ± 9, 158 ± 7, and 59 ± 38 GPa at 298, 700, and 1100 K, respectively.

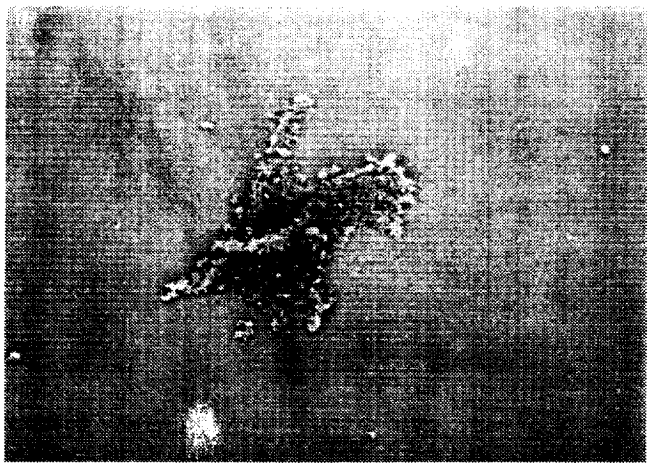

(*a*)

(*b*)

Fig. 7—(*a*) Surface morphology of Al_2O_3 fiber etched from FeAl + B, and (*b*) fracture initiation site of Al_2O_3 etched from FeAl + B.

Table III. Tensile Properties of Al_2O_3/FeAl + B

Temperature (K)	σ_{UTS} (MPa)	σ_{el} (MPa)	E (GPa)	ε_{UTS} (Pct)	ε_{el} (Pct)	ε_f (Pct)	V_f (Pct)
298	637	107	255	0.42	0.04	0.42	27
	676	104	230	0.50	0.04	0.50	26
	537	116	189	0.36	0.07	0.36	27
	584	—	185	0.50	—	0.50	18
700	533	—	279	3.8	—	4.1	37
	526	—	265	2.0	—	2.0	30
	606	—	287	3.0	—	3.1	30
1100	147	—	—	2.0	—	2.4	31
	87	—	55	1.2	—	4.2	27
	117	—	47	2.6	—	2.8	18
	97	—	87	2.3	—	2.8	19

2. *Al_2O_3/FeAl + B*

Representative composite stress-strain curves are compared to those for hot-pressed monolithic FeAl + B in Figure 9, and the individual mechanical property values for each composite tested are listed in Table III. The room-temperature stress-strain curves consisted of a linear elastic region followed by a slightly curved region up to the failure stress. The room-temperature UTS averaged 608 ± 97 MPa with failure strains ranging from 0.36 to 0.50 pct. At

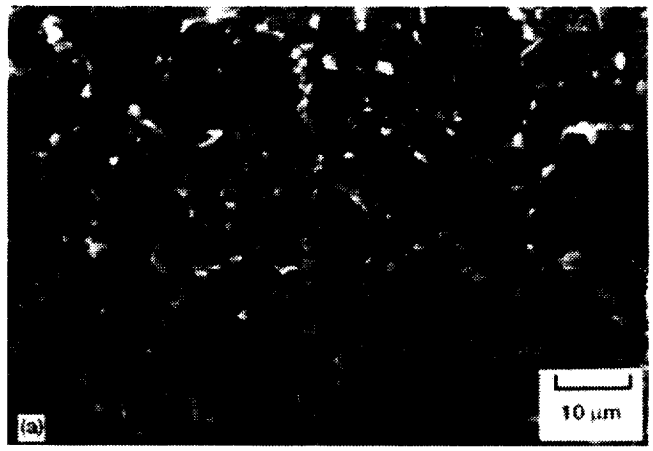

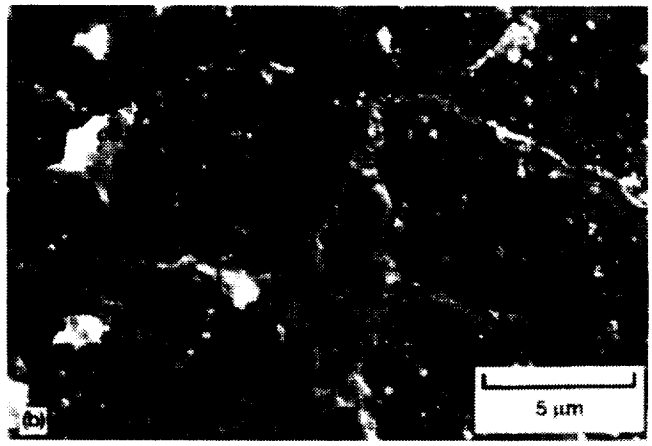

Fig. 8—Surface morphology of Al_2O_3 extracted from FeCrAlY showing (*a*) adherent particles rich in Cr and Al and deficient in Fe and (*b*) a Y-rich phase in grooved areas and on the surface of Al_2O_3 fiber.

700 K, there was an initial elastic portion of the curve after which there were many sharp drops and increases in stress, resulting in a serrated appearance to the stress-stain curve. Each sharp drop in stress was accompanied by an audible click, which was believed to be fiber breakage. At 700 K, failure occurred at the UTS with a failure strain that ranged from 2.0 to 4.1 pct. Two types of stress-strain curves were generated at 1100 K. The first type was similar to the 700 K curves in which there were gradual increases in strength until the composites failed at the UTS. The second type of stress-strain curve contained a large load drop at the UTS followed by gradual failure. Final fracture occurred for both cases between 2.4 and 4.2 pct strain.

The Al_2O_3/FeAl + B composites accumulated large elongations to failure at 700 and 1100 K. In order to attain these large strains, the fibers failed and the low interfacial shear strengths allowed the broken fibers to slide apart. Large voids formed between the broken fiber ends (Figure 10). The low interfacial bond strength also resulted in large amounts of fiber pullout at all test temperatures (Figure 11). The maximum measured pullout was 1100 μm at room temperature, 525 μm at 700 K, and 780 μm at 1100 K.

3. *Acoustic emission*

Acoustic emission activity was not detected during the initial linear region, which extended to 0.15 pct strain (Fig-

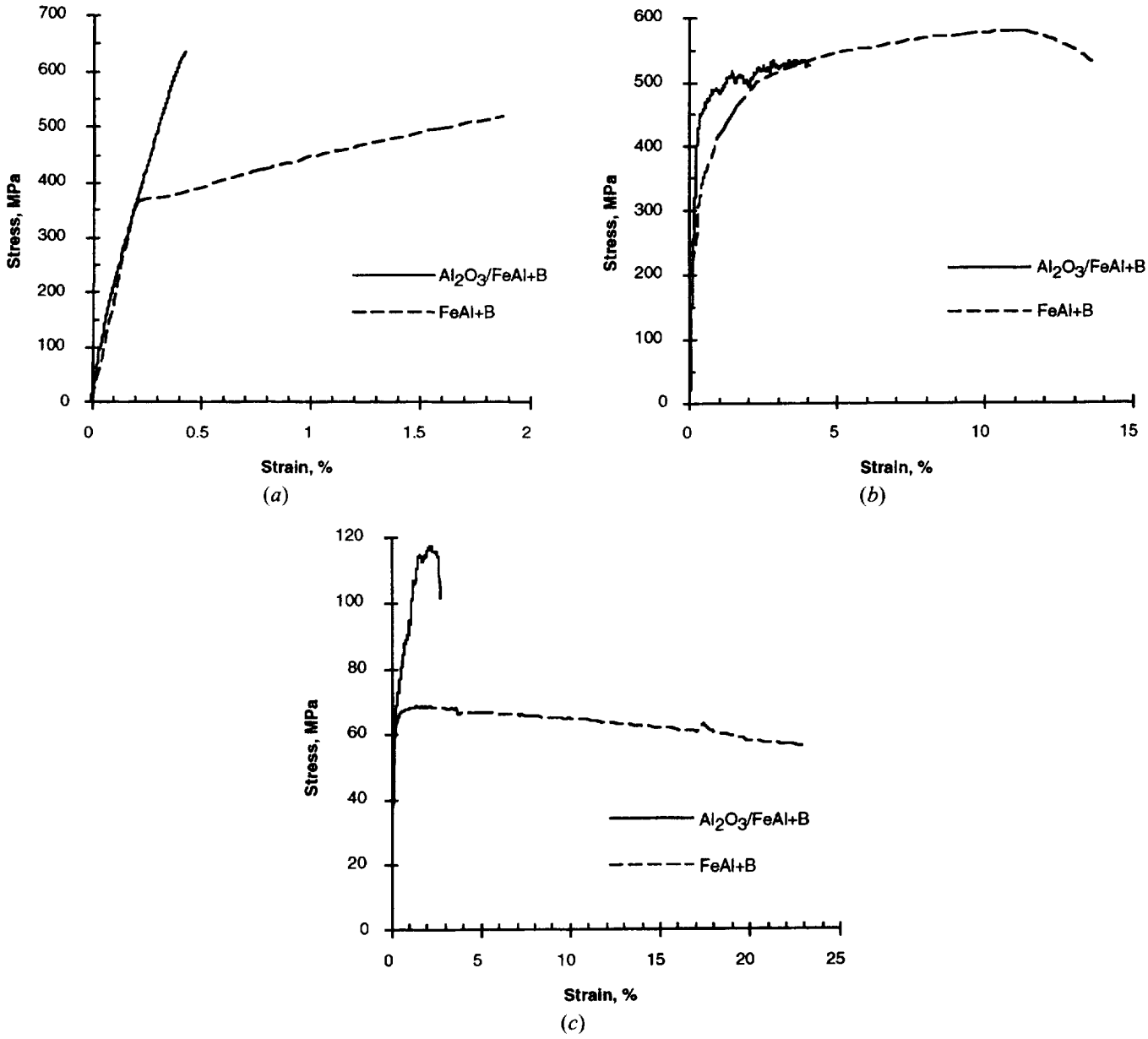

Fig. 9—Typical FeAl + B monolithic and Al_2O_3/FeAl + B composite stress-strain curves at (*a*) 298 K, (*b*) 700 K, and (*c*) 1100 K.

ure 12). A significant level of AE activity was recorded after 0.17 pct strain (Figure 12(c)). The mode of the recorded hits had a high amplitude, 98 dB, which indicates that the activity was primarily fiber fracture. As shown in the source location plot of Figure 12, AE events occurred in a random manner throughout the gage section and the composite failed within the cross section having the largest number of acoustic events. Confirming that the AE activity was primarily fiber breakage, a few random cracks were observed in metallographic sections along the length of the fibers, but extensive fiber cracking along individual fibers was not observed (Figure 10).

The first Al_2O_3 fiber failure in FeAl + B occurred at 0.17 percent strain at room temperature. Ignoring residual stresses and assuming isostrain conditions, the stress on the fibers at 0.17 pct strain was calculated to be 768 MPa using an elastic modulus of 452 GPa for Al_2O_3.[8] Although the average strength of the Al_2O_3 fibers etched from FeAl + B was 1413 MPa at room temperature, the lowest strength measured was 836 MPa. This indicates that the strengths of fibers in the composite were essentially the same as the strengths of fibers etched from the composite and tested in single-fiber tensile tests.

E. *FeCrAlY and Al_2O_3/FeCrAlY Tensile Behavior*

1. *FeCrAlY*

Typical stress-strain curves for monolithic FeCrAlY are shown in Figure 13. At room temperature, the FeCrAlY specimens yielded at an average of 528 ± 23 MPa and strain hardened to an average UTS of 670 ± 19 MPa where failure occurred. At 700 K, FeCrAlY strain hardened to an average UTS of 465 ± 125 MPa which generally occurred at 50 pct of ε_f. Gradual strain softening occurred until the

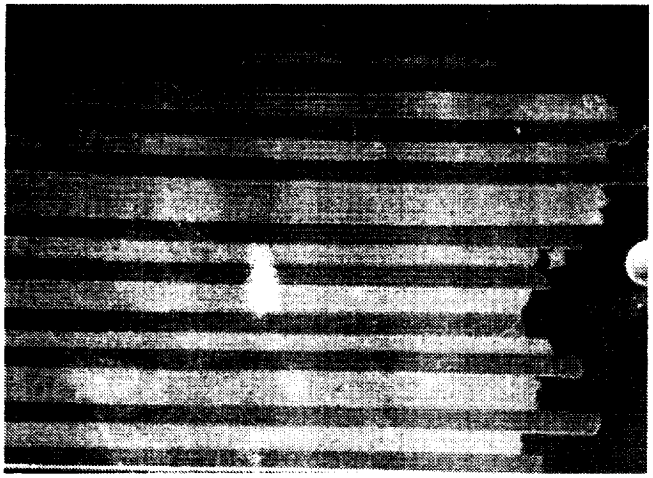

(*a*)

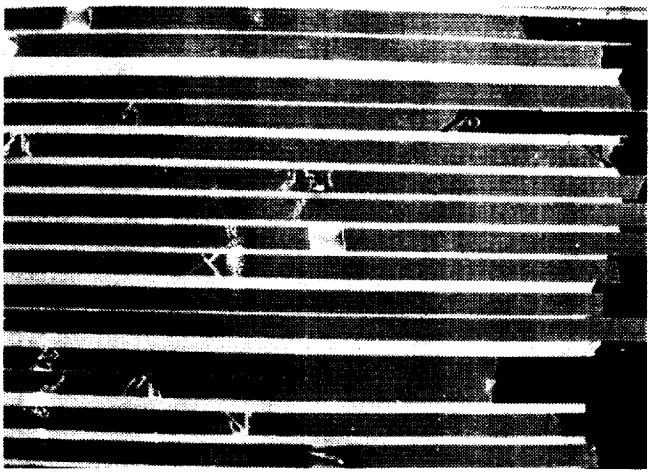

(*b*)

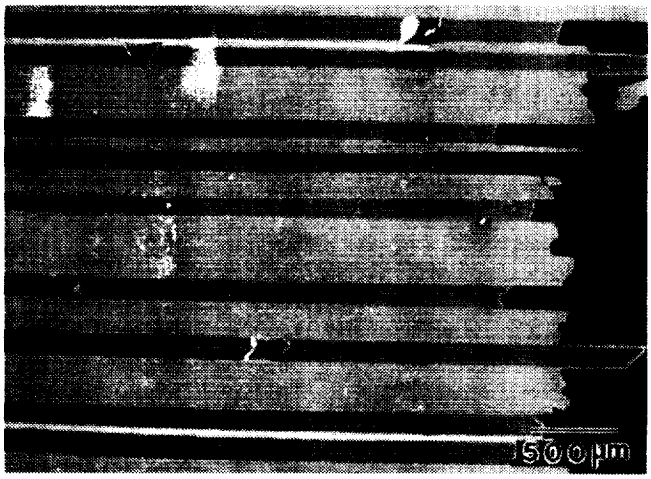

(*c*)

Fig. 10—Longitudinal sections of fractured tensile specimens of Al203/FeAl + B tested at (*a*) 298 K, (*b*) 700 K, and (*c*) 1100 K showed few fiber cracks.

end of the tests where the rate of strain softening increased. At 1100 K, the UTS of FeCrAlY, 51 ± 16 MPa, was only slightly higher than the yield strength, 48 ± 16 MPa, and strain softening occurred throughout the majority of the

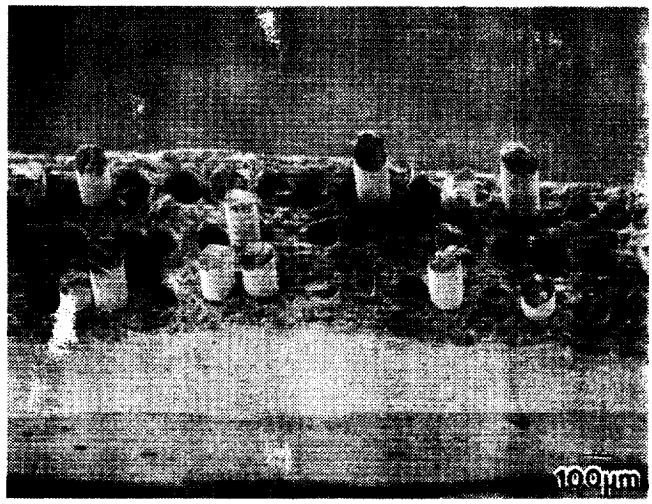

Fig. 11—Fracture surfaces of Al203/FeAl + B show extensive fiber pullout at all test temperatures.

tests. The elastic moduli averaged 234 ± 10, 195 ± 21, and 63 ± 25 GPa at 298, 700, and 1100 K, respectively.

2. *Al_2O_3/FeCrAlY*

Al_2O_3/FeCrAlY composites were tensile tested at 298, 700, and 1100 K, and a compilation of the individual composite tensile properties is given in Table IV. The room-temperature stress-strain curves consisted of an initial linear region followed by a slightly curved region up to the UTS of the material (Figure 13(a)). A large load drop occurred at the UTS, which averaged 739 ± 80 MPa, followed by a plateau maintained until failure. At 700 K, the initial portion of the curve was essentially linear but not entirely smooth (Figure 13(b)). It is believed that fiber breaks during the elastic portion resulted in striations in the curve. Similar to the room-temperature tests, a load drop coincided with the UTS and was followed by some elongation to failure. At 1100 K, the specimens typically failed outside of the extensometer such that the elongations to failure were not obtained. The stress-strain curve in Figure 13(c) is shown only up to the UTS. Serrations in the stress-strain curve indicate that fibers fractured at stresses as low as 10 MPa. One Al_2O_3/FeCrAlY specimen was tested at 1100 K under load control. This sample failed at 172 MPa with a corresponding strain of 0.10 pct (Table IV).

The polished longitudinal sections of Al_2O_3/FeCrAlY fracture surfaces show fibers broken throughout the gage sections, but higher concentrations of broken fibers were localized to the failure site (Figure 14). At 1100 K, one tensile specimen did not completely separate, although no apparent load was carried at the end of the test (Figure 14(c)). The fibers were broken completely across the longitudinal section, and some had significant separation; however, the matrix was still intact and exhibited localized necking. The fracture surfaces at all test temperatures exhibited little fiber pullout (Figure 15).

3. *Acoustic emission*

The results of the room-temperature tensile test of the Al_2O_3/FeCrAlY specimen tested with AE are shown in Figure 16. The linear region of the stress-strain curve extended to 0.08 pct strain. Acoustic activity started at 0.16 pct strain, nearly identical to the strain at which fibers started to fail

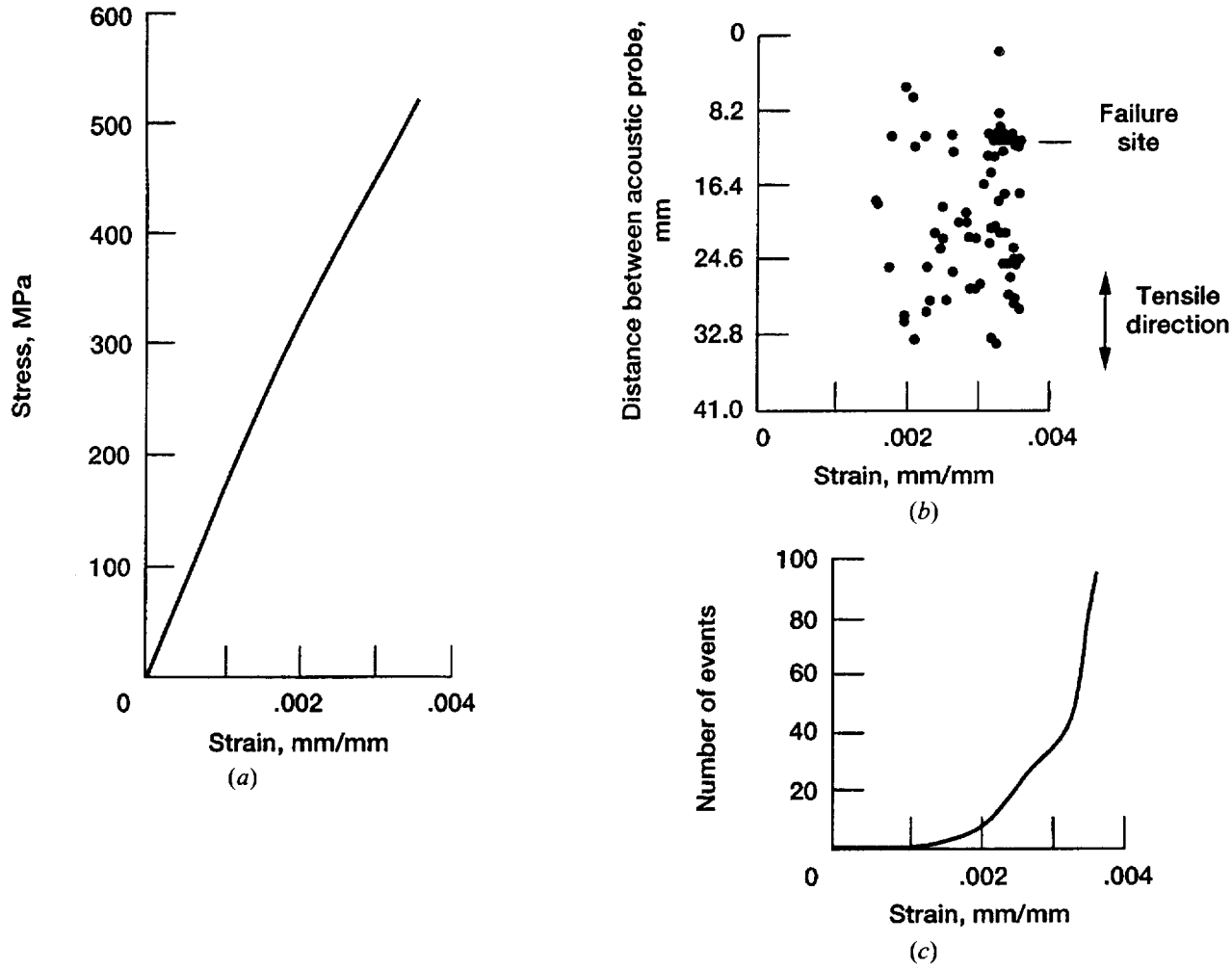

Fig. 12—(*a*) The stress-strain curve for the Al_2O_3/FeAl + B sample which was tested with AE. (*b*) Fibers broke throughout the gag section, with failure occurring at the cross section with the largest number of fiber breaks. (*c*) Fibers started failing at 0.17 pct strain, but the rate of fiber fracture increased at 0.32 to 0.37 pct where failure occurred.

in the Al_2O_3/FeAl + B sample. As with Al_2O_3/FeAl + B, the majority of the AE activity was at high decibel levels, which correspond to fiber breakage. The fibers failed in a random manner over the length of the sample up to 0.37 pct strain, which was the strain at which the UTS occurred for this sample. After the load drop, AE results indicated that multiple fiber cracks occurred in an area localized to the failure region. The majority of AE events occurred after reaching the UTS (Figure 16) due to fibers breaking into shorter and shorter segments until final failure occurred at a strain of 1.3 pct. Failure occurred in the cross section where the most fibers failed prior to and following the UTS. The polished longitudinal section (Figure 14) of the failed tensile specimen confirmed the localization of the fiber cracking.

IV. DISCUSSION

Several composite properties affect the failure mode of the composite,[9,10] but the two of most relevant in these composite systems are scatter in fiber strength and interfacial bond strength. A wide scatter in fiber strength promotes cumulative failure,[9] described as the gradual accumulation of fiber breaks prior to composite failure. As the weakest fibers fail, neighboring fibers are typically strong enough to bear an increased load.[11] In contrast, composites fail in a noncumulative manner when failure of only a few fibers results in composite failure. The etched-out Al_2O_3 fibers had a wide scatter in fiber strength, characterized by a low Weibull modulus (m = 5), which resulted in a cumulative failure mode for both composite systems.

The significantly different interfacial shear strengths of the two composite systems impacted the tensile behavior. Interfacial shear strengths are directly related to the critical length of fiber, l_c. Stresses gradually build up in the broken fibers from the fiber ends to a distance 0.5 l_c.[12] With weak interfacial shear strengths, l_c is long and the load bearing efficiency of the fiber is reduced from the broken end to a distance of 0.5 l_c.[12] Additionally, the fibers can debond and slide at the interface in the vicinity of fiber cracks. Composites with strong interfacial shear strengths have short critical lengths, and broken fibers have a high load-bearing capacity. However, stress concentrations, which develop in neighboring fibers, can counterbalance the effect of high load-bearing efficiency.

The interfacial bond and frictional strengths were low for Al_2O_3/FeAl + B composites at room temperature and were presumed to be even lower at elevated temperatures as the

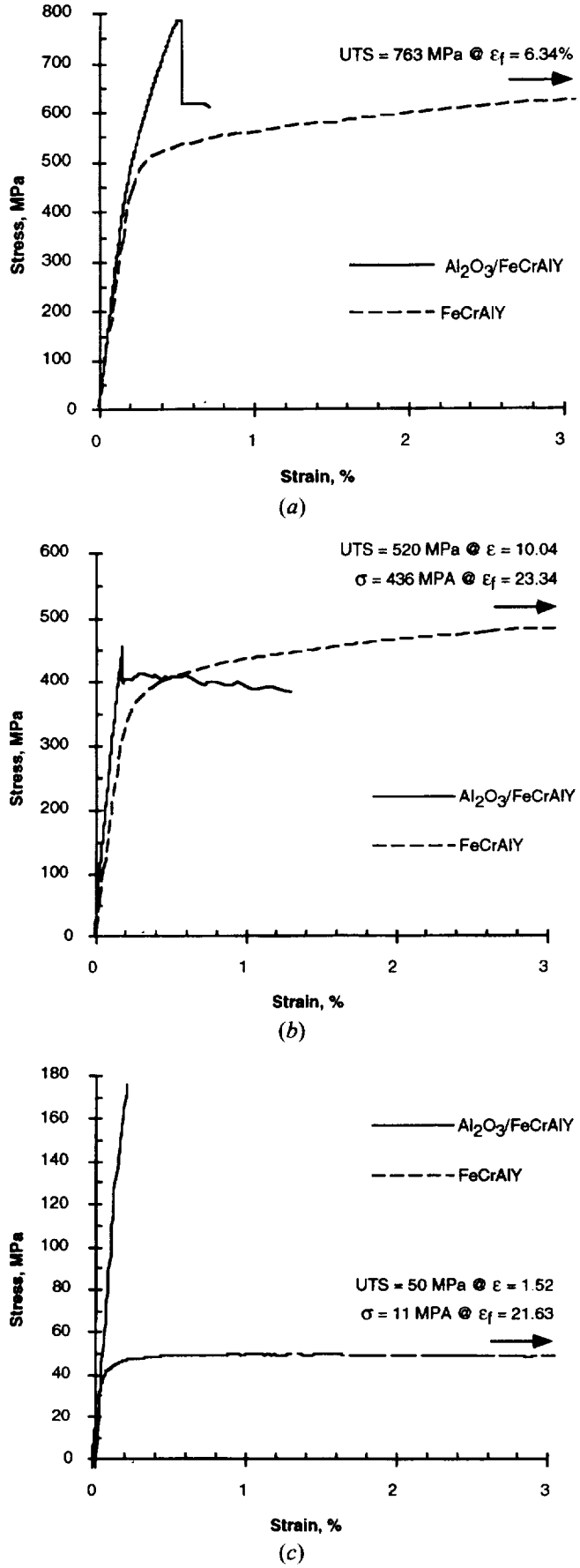

Fig. 13—Representative stress-strain curves for FeCrAlY and Al203/FeCrAlY at (*a*) 298 K, (*b*) 700 K, and (*c*) 1100 K.

Table IV. Tensile Properties of Al_2O_3/FeCrAlY

Temperature (K)	σ_{UTS} (MPa)	σ_{el} (MPa)	E (GPa)	ε_{UTS} (Pct)	ε_{el} (Pct)	ε_f (Pct)	V_f (Pct)
298	787	310	291	0.50	0.11	0.70	25
	656	340	256	0.41	0.14	1.14	22
	819	190	270	0.48	0.06	0.62	25
	755	245	288	0.41	0.09	1.97	25
	701	240	315	0.37	0.09	1.78	
	515	380	310	0.18	0.13	0.30	46
	646	365	300	0.27	0.13	0.32	45
	810	440	351	0.31	0.13	0.37	45
	785	295	308	0.44	0.11	0.76	22
700	454	—	298	0.18	—	1.30	30
	470	—	282	0.20	—	1.16	30
	450	—	257	0.20	—	0.39	34
	468	—	—	0.18	—	0.53	34
1100	143	—	—	0.08	—	—	36
	137	—	—	0.18	—	—	25
	176	—	—	0.20	—	—	25
	122	—	—	0.07	—	—	32
	172	—	—	0.10	—	0.10	27

residual clamping stresses would be relieved. Room-temperature AE data show that the fibers failed randomly throughout the gage section until a significant number failed within a cross section and failure occurred catastrophically from overload. The influence of the low interfacial shear strengths was more pronounced at 700 and 1100 K. As each fiber failed, a small load drop occurred. As the loads were transferred to neighboring fibers, the load would slowly increase until another fiber would fail, resulting in a serrated appearance of the stress-strain curves (Figure 9). The low interfacial strengths allowed fiber sliding in the matrix at the elevated temperatures, resulting in the large elongations to failure. As discussed subsequently, the composite UTS values at 1100 K were less than estimated using the rule of mixtures (ROM). At 1100 K, composite strength was apparently limited by the lack of load transfer.

The failure mechanisms for Al_2O_3/FeCrAlY composites were similar at all test temperatures. At room temperature, AE data show that the fibers failed in a random manner throughout the gage section of the composite. When sufficient fibers had failed in one cross section, the composite could no longer carry an increase in the load and the UTS was reached. However, due to the constant cro ead speed test method, the ductility of the matrix, and the fairly strong interfacial bond strength, the composites accumulated strain at a reduced load after the UTS was achieved. The load dropped to a level at which the cross section with the most fiber breaks could sustain. The fibers local to the failure region had higher than normal stress concentrations due to the surrounding broken fibers. These fibers broke into successively shorter segments due to the strong interfacial bond strength and corresponding short critical fiber lengths. Thus, Al_2O_3/FeCrAlY failed in a cumulative, but not catastrophic, manner.

The simplest prediction of the UTS can be calculated with the ROM equation[13] using the strength of the etched-out fibers and the strength of the matrix at the failure strain of the fiber. A more sophisticated model for predicting the ultimate strength, σ_{UTS}, of a composite was developed by Curtin[14] and is given below:

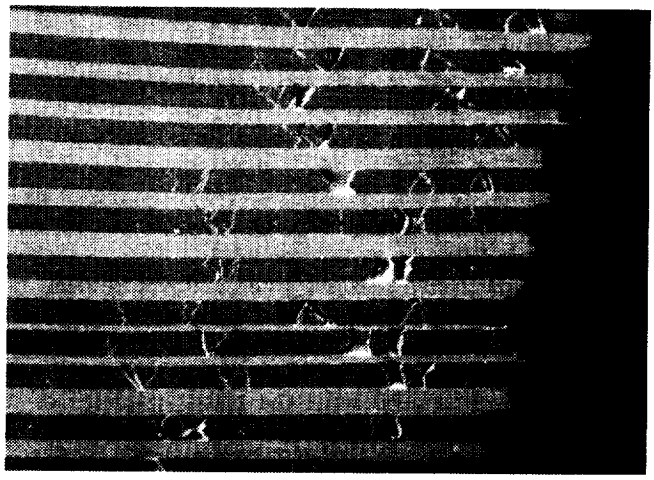

(*a*)

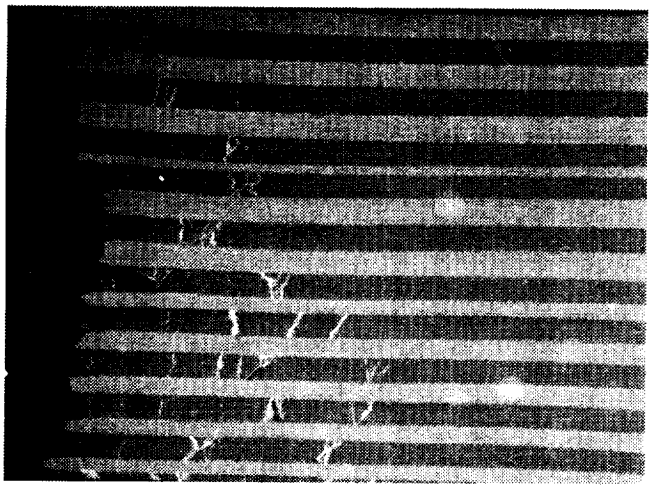

(*b*)

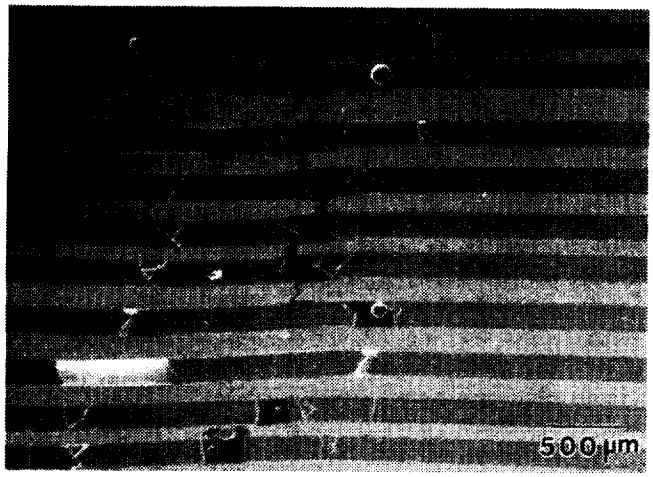

(*c*)

Fig. 14—Longitudinal section of fracture tensile specimens of Al203/FeCrAlY tested at (*a*) 298 K, (*b*) 700 K, and (*c*) 1100 K shows fiber cracking localized to the failure region.

$$\sigma_{UTS} = V_f[(\frac{2}{m+2})^{\frac{1}{m+1}}(\frac{m+1}{m+2})][\frac{\sigma_f^m \tau_f L_0}{r}]^{\frac{1}{m+1}} + (1-V_f)\sigma_y$$

where V_f is the fiber volume fraction, m is the Weibull

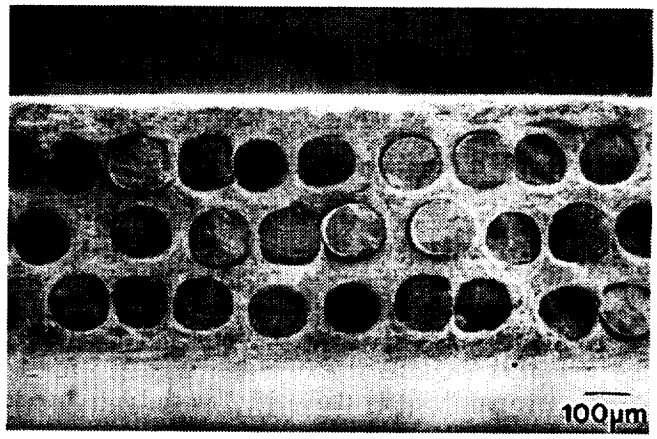

Fig. 15—Fracture surfaces of Al203/FeCrAlY show little fiber pull-out at all test temperatures.

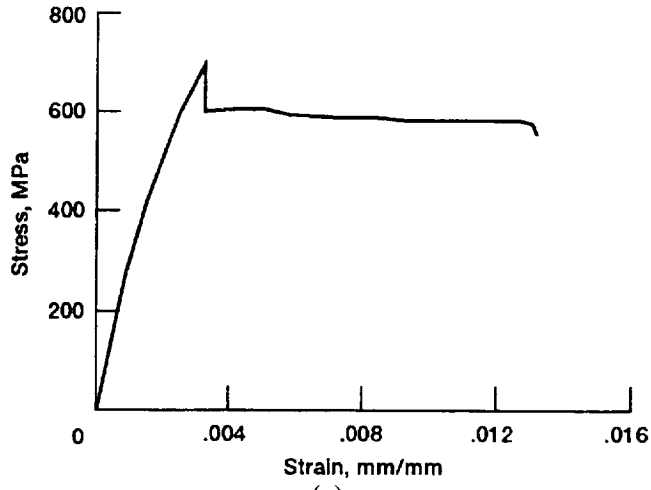

(*a*)

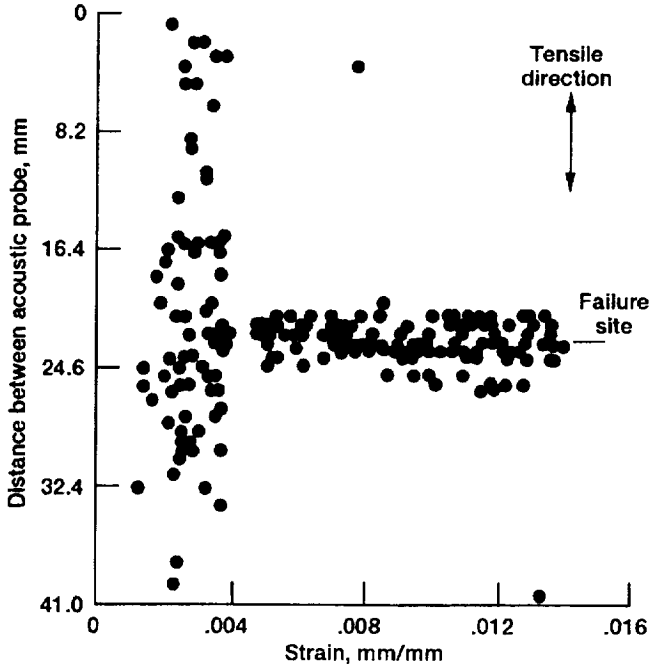

(*b*)

Fig. 16—(*a*) The stress-strain curve for the Al203/FeCrAlY sample tested with AE at room temperature. (*b*) Fibers failed in random locations up to the σ_{UTS} after which they failed localized to the failure region.

modulus, σ_f is the average fiber strength at gage length L_0, τ_f is frictional shear stress, r is the fiber radius, and σ_y is the yield strength of the matrix. Curtin's model was not used to predict the elevated temperature strength of Al_2O_3/FeAl + B, as the required properties were not well characterized at elevated temperatures. The true gage length of fibers tested at elevated temperatures was not known but was estimated to be 5 mm.

Simple ROM calculations came within 5 pct of the experimental UTS values for Al_2O_3/FeAl + B at room temperature, but Curtin's model[14] underestimated the experimental values by 16 pct. At 700 K, the UTS values of the Al_2O_3/FeAl + B composites were substantially higher than predicted by the ROM. The composites tested at 700 K were fabricated using fiber with higher as-received strength (more recently purchased fiber). It is possible that the residual fiber strength after processing was higher for these composites than for the composite which was used for fiber etch-out and testing. Additionally, ROM incorporates the strength of the matrix at the failure strain of the fiber; however, the composites failed at significantly higher strains and the matrix could have experienced work hardening. At 1100 K, the experimental UTS values were significantly lower than predicted by ROM and the fibers failed at lower loads than expected based on single-fiber tests of etched-out fibers. While the low interfacial strength of this composite system most likely resulted in inefficient load transfer, strengthening was achieved, as the composite failed at a substantially higher UTS than the monolithic at 1100 K, 112 ± 2 MPa, and 67 ± 4 MPa, respectively.

The UTS of the six Al_2O_3/FeCrAlY specimens, with V_f averaging 0.24, were fairly accurately predicted by both ROM and Curtin's model, within 5 pct at room temperature. The average room-temperature UTS of these six specimens was 751 ± 64 MPa, approximately 100 MPa higher than the average UTS for the monolithic specimens (Table IV). At 700 and 1100 K, the ROM was a better prediction, as the experimental values were within 5 pct of the ROM but only within 15 pct of the estimated strength using Curtin's model.

The UTS values of the high V_f specimens, tested at 298 K, were overestimated by both ROM and Curtin's model. The high fiber volume fraction Al_2O_3/FeCrAlY specimens, which were all from one composite plate (plate A in Table II), had a low interfacial bond strength. While these low interfacial strengths were used in Curtin's model, sufficiently low UTS values were still not obtained. The increased volume of fibers could have resulted in matrix yielding during cooldown from the fabrication temperature and could have contributed to the low UTS values. However, the composite σ_{el} indicated that the matrix did not yield at anomalously low applied loads.

It should be emphasized that the major cause for the unacceptably low composite UTS values at all test temperatures is fiber strength degradation after processing. The UTS values of the composites were generally not substantially higher than the UTS of the monolithic specimens at room temperature and 700 K due to work hardening in the monolithic specimens. However, a comparison of composite and monolithic strength at ε_{UTS}^c (strain at the composite UTS) shows an improvement of composite strength over monolithic strength in most cases. A significant increase in composite UTS values compared to monolithic UTS occurred only at 1100 K, where matrix work hardening was not a factor. At elevated temperatures, metal matrix composites depend on the fiber for adequate strength. While the composite σ_{UTS} values were improved over the monolithic σ_{UTS} at 1100 K, the fibers failed at low loads and the composites failed at very low strains. The strength of Al_2O_3 fiber must be maintained if Al_2O_3 fiber reinforced metal matrix composites are to become useful.

Besides increasing strength, ceramic fibers in metal matrices can increase stiffness and the elastic modulus of a composite can be predicted based on ROM.[13] The room-temperature elastic modulus of the FeAl + B matrix averaged 203 ± 8 GPa while the elastic modulus of the composite ranged from 185 to 255 GPa, only 75 to 85 pct of ROM. The deviations from ROM modulus could have been a result of a number of factors, including a tensile residual stress state in the matrix, broken fiber ends in the gage section, and weak interfacial bond strengths. At 700 K, the Al_2O_3/FeAl + B composite specimens were significantly stiffer than the matrix having a modulus of elasticity averaging 272 GPa, while at 1100 K, the elastic moduli were only 50 pct of the ROM estimates. At elevated test temperatures, the clamping stresses around the fiber from the residual stresses in the matrix are generally relaxed and the interfacial shear strength decreases. The efficiency of load transfer at elevated temperatures may have been low enough to affect the measured elastic modulus. The moduli of elasticity for Al_2O_3/FeCrAlY composites were equivalent to the expected ROM values[13] at all test temperatures.

Residual stresses can affect the elastic limit of the composite, σ_{el}^c. The values of σ_{el}^c, listed in Tables III and IV for room-temperature tests, could not be obtained for the elevated temperature tests due to the early onset of fiber breakage. The σ_{el}^c has been shown to coincide with matrix yielding in some metal matrix composites.[15,16] Assuming isostrain conditions, the applied stress in the matrix (σ_A^m) at the elastic limit can be calculated as follows:[16]

$$\sigma^m{}_A = E_m \varepsilon^c{}_{el}$$

where ε_{el}^c is the strain of the composite at the elastic limit and E_m is the elastic modulus of the matrix. Assuming the bend in the stress-strain curve corresponds to matrix yielding, the FeAl + B in the composites yielded at an applied stress of 100 MPa, significantly below the elastic stress limit of 300 MPa for monolithic specimens (σ_{el}^m) at room temperature. The FeCrAlY matrix in the composites with $V_f = 0.25$ yielded at an applied stress of 240 MPa, which again was significantly lower than the average $\sigma_{el}^m = 416$ MPa for FeCrAlY monolithic samples at room temperature. Besides matrix yielding, fiber breakage could contribute to a change in elastic modulus; however, AE results indicated that fiber breakage did not begin until a strain of 0.16 pct, well after the σ_{el}^c. Microstructural examination of the matrix in the composites would need to be performed to ascertain that matrix yielding did not occur during cooldown from the fabrication temperature. However, if the bend in the stress-strain curve was due to matrix yielding, the difference between the σ_{el}^m and the applied stress of the matrix in the composite is most likely due to residual stresses that have developed in the composite during cooldown from the

fabrication temperature.[16] Using this assumption, the residual stress at room temperature was calculated to be 200 MPa in the Al_2O_3/FeAl + B composites and approximately 175 MPa in the 0.25 V_f Al_2O_3/FeCrAlY samples. These results agree with the fact that the ΔCTE is greater between Al_2O_3 and FeAl + B (average ΔCTE ≈ 16 * 10^{-6}/K)[17] than between Al_2O_3 and FeCrAlY (average ΔCTE ≈ 6 * 10^{-6}/K).[17]

While not a part of this study, the response of these composites to thermal cycling has been studied previously,[18] and the results have an impact on determining the feasibility of these composites for high-temperature applications. The composites were cycled from room temperature to 1100 K for 1000 cycles in air. After cycling, the Al_2O_3/FeAl + B system had protruding fibers and holes from which fibers were displaced by up to a few millimeters at both ends of the coupons.[18] The Al_2O_3 fibers had debonded from the FeAl + B matrix, and the extension of the fibers from the matrix was attributed to a ratcheting type phenomenon due to the release and tightening of CTE mismatch-induced mechanical clamping forces.[18] By comparison, the Al_2O_3/FeCrAlY sample survived 1000 cycles with no damage.[18]

The strength degradation of Al_2O_3 fibers during processing of both FeAl + B and FeCrAlY matrix composites was detrimental to the tensile properties of the composites. A study was initiated to determine the mechanisms contributing to the strength loss of the Al_2O_3 fibers in these and other matrices.[6] Four mechanisms were proposed as contributing to the fiber strength degradation: matrix reaction, binder reaction, residual stresses, and hot-pressing pressure. For the FeCrAlY-type alloys, both Y and Cr were identified in reaction products, adherent to the fiber surface, which appeared to be strength-limiting flaws. The four mechanisms are inter-related and difficult to separate, but matrix reaction was determined to be the dominant mechanism for the FeCrAlY matrix composites. Incomplete burn-off of the PMMA binder used in the powder cloth technique resulted in a carbon residue on the fibers etched from NiAl and FeAl matrix composites.[6] Recently, a different binder has been used in the powder cloth technique such that no C residue is found on the fibers etched from FeAl + B composites. These fibers had an average strength of 2348 MPa after etching from the composite. This is an important result, as it suggests that the fibers can be processed without prohibitively high strength loss; however, the good strength retention may be due to the poor bond between Al_2O_3 and FeAl + B. Despite these recent encouraging results, work in the area of FeAl + B matrix composites has been discontinued due to the high CTE of FeAl + B and the poor bonding between Al_2O_3 and FeAl + B.

V. SUMMARY AND CONCLUSIONS

The low interfacial bond strength of Al_2O_3/FeAl + B resulted in catastrophic failure at room temperature, but the composites failed in a noncatastrophic manner with significant elongations to failure at elevated temperatures. The UTS values of Al_2O_3/FeAl + B composites were accurately predicted by ROM strength estimates at room temperature but were below predictions at 1100 K due to the low interfacial strength of Al_2O_3/FeAl + B. The test methodology, ductility of the matrix, and strong interfacial bond strength contributed to the Al_2O_3/FeCrAlY composites failing in a noncatastrophic manner at all test temperatures. The UTS values of the Al_2O_3/FeCrAlY specimens, with lower V_f, were predictable by both ROM and Curtin's theory. The degradation of Al_2O_3 fiber strength during processing was detrimental to composite tensile properties. The degradation of Al_2O_3 fiber strength was a result of incomplete binder burn-off in the Al_2O_3/FeAl + B system and fiber/matrix reaction in the Al_2O_3/FeCrAlY system. If Al_2O_3 fiber reinforced metal matrix composites are to be viable, the integrity of the fibers must be maintained during processing. In recent experiments, fiber strength degradation for Al_2O_3/FeAl + B was minimized when C contamination was eliminated; however, this composite system was still determined to be unfeasible due to low interfacial shear strengths and large mismatch in CTE. A diffusion barrier coating and/or matrix composition variations would be required in the Al_2O_3/FeCrAlY composite system to prevent matrix reactions with the fiber during processing and elevated temperature service. Single-crystal Al_2O_3 fibers are very sensitive to surface defects, and the most promising option for superalloy matrix composites may be to use a different fiber, one that is less sensitive to surface flaws. Unfortunately, the choice of available fibers is extremely limited. Finally, AE detection during tensile testing was validated as a useful tool for determining the tensile failure mechanisms of Fe-based matrix composites.

REFERENCES

1. M.S. Madhukar and J. Awerbuch: *Composite Materials: Testing and Design*, 7th Conf., ASTM STP-893, J.M. Whitney, ed., ASTM, Philadelphia, PA, 1986, pp. 337-67.
2. J.G. Bakuckas, Jr., W.H. Prosser, and W.S. Johnson: NASA TM-107742, 1993.
3. J.W. Pickens, R.D. Noebe, G.K. Watson, P.K. Brindley, and S.L. Draper: NASA TM-102060, 1989.
4. J.I. Eldridge: NASA TM-105341, 1991.
5. J.I. Eldridge and B.T. Ebihara: *J. Mater. Res.*, 1994, vol. 9, pp. 1035-42.
6. S.L. Draper and I.E. Locci: *J. Mater. Res.*, 1994, vol. 9 (6), pp. 1397-1411.
7. A. Sayir: Paper presented at *15th Annual Conf. on Composites and Advanced Ceramics*, Cocoa Beach, FL, 1991.
8. W.B. Hillig: *Tailoring Multiphase and Composite Ceramics*, R.E. Tressler, G.L. Messing, C.G. Pantano, and R.E. Newnham, eds., Plenum Publishing Corp., New York, NY, 1986, pp. 697-712.
9. S. Ochiai and K. Osamura: *J. Mater. Sci.*, 1988, vol. 23, pp. 886-93.
10. S. Ochiai and K. Osamura: *Metall. Trans. A*, 1990, vol. 21A, pp. 971-77.
11. C. Zweben: *AIAA J.*, 1968, vol. 6, pp. 2325-31.
12. A. Kelly and W.R. Tyson: *J. Mech. Phys. Solids*, 1965, vol. 13, pp. 329-50.
13. D.L. McDanels, R.W. Jech, and J.W. Weeton: *Trans. AIME*, 1965, vol. 233, pp. 636-42.
14. W.A. Curtin: *Composites*, 1993, vol. 24 (2), pp. 98-102.
15. B.A. Lerch: NASA TM-103760, 1991.
16. P.K. Brindley, S.L. Draper, J.I. Eldridge, M.V. Nathal, and S.M. Arnold: *Metall. Trans. A*, 1992, vol. 23A, pp. 2527-40.
17. B.J.M. Aikin, D.W. Petrasek, and S.L. Draper: NASA CP-19117, 1993.
18. D.J. Gaydosh, S.L. Draper, J.I. Eldridge, and P. Tsui: NASA CP-10051, 1990.